Journal of Power Sources 241 (2013) 196–202

Contents lists available at SciVerse ScienceDirect

Journal of Power Sources

journal homepage: www.elsevier.com/locate/jpowsour

A high power density single flow zinc–nickel battery with three-dimensional porous negative electrode

Yuanhui Cheng [a,b], Huamin Zhang [a,**], Qinzhi Lai [a,*], Xianfeng Li [a], Dingqin Shi [a], Liqun Zhang [a,b]

[a] Division of Energy Storage, Dalian Institute of Chemical Physics, Chinese Academy of Sciences, 457 Zhongshan Road, Dalian 116023, PR China
[b] University of Chinese Academy of Sciences, Beijing 100039, PR China

HIGHLIGHTS

- Three-dimensional porous electrode is first introduced to ZNBs.
- The utilized electrode area and potential distribution has been studied.
- An EE (80.1%) is obtained at 80 mA cm^{-2}, which is the highest value ever reported.
- The power density is improved nearly four times to 83 W Kg^{-1}.

ARTICLE INFO

Article history:
Received 8 March 2013
Received in revised form
19 April 2013
Accepted 23 April 2013
Available online 2 May 2013

Keywords:
Flow batteries
Electrochemistry
Energy storage
Porous electrode
Zinc

ABSTRACT

Low power density (operated current density) is one critical obstacle to the development of single flow zinc–nickel batteries (ZNBs). Three-dimensional porous nickel foams (NFs) are first introduced to ZNBs to improve power density. The relationship between utilized electrode area, potential distribution and operated current density has been studied. A high coulombic efficiency (97.3%) and energy efficiency (80.1%) are obtained at 80 mA cm^{-2} over 200 cycles, which is the highest value ever reported for ZNBs. The power density is improved nearly fourfold to 83 W kg^{-1}. The results indicate that three-dimensional porous electrodes are more suitable as negative electrodes for ZNBs under high operated current densities. This provides an effective way to improve power density of ZNBs and will arouse a new revolution in the development of flow batteries.

1. Introduction

Exigent demand for energy has attracted the attention on the applications of clean energy resources. But these clean energy forms (e.g., solar, wind, nuclear and tide) are usually fluctuant and dispersed, which make them difficult to integrate into the electric grid or utilize continuously. Hence, energy storage becomes a critical technology for the applications of clean energy resources [1,2]. Energy storage mainly focuses on electrochemical systems due to its wide range of storage capacity and no regional condition confine [3,4]. Among them, flow battery (FB) is one of the most promising candidates due to its high storage efficiency, excellent capability, security, reliability and flexible operation [5,6]. Thus, various flow battery systems have sprung up attributed to the interest in both researches and commercial applications [7–15]. One of the most promising systems, zinc–nickel batteries are of high open circle potential (1.705 V) and high energy density (above 65 Wh kg^{-1}) [15]. Furthermore, ZNBs are made from cheap, non-toxic materials that are inherently safe. No membrane is needed, which simplifies the battery system and reduces the integration cost. But together with other demonstrated systems, they are nearly all operated at current densities below 40 mA cm^{-2}. For instance, the operated current density of soluble lead acid batteries (SLABs) [14], zinc-bromine batteries (ZBBs) [9,16] and zinc–nickel batteries (ZNBs) [17,18] is below 20 mA cm^{-2}. The polysulfide–bromine battery (PSB) reaches to 40 mA cm^{-2} [13], but still limits the quick response for energy conversion. The power density, which is associated with the operated current density, has a significant influence on energy conversion rate and the integration cost. Thus, increasing power density of ZNBs without compromising battery performance is an effective strategy to meet the requirements for commercialization.

* Corresponding author. Tel./fax: +86 (0) 411 84379580.
** Corresponding author.
E-mail address: qinzhilai@dicp.ac.cn (Q. Lai).

0378-7753/$ – see front matter © 2013 Elsevier B.V. All rights reserved.
http://dx.doi.org/10.1016/j.jpowsour.2013.04.121

In ZNBs, both anolytes and catholytes are the high soluble alkaline zincate solutions pumped through a single pump. During charge, metallic zinc deposits at the negative electrode at −1.216 V vs. the normal hydrogen electrode (NHE), whereas $Ni(OH)_2$ undergoes solid-phase transformation to NiOOH at positive electrode at 0.49 V vs. NHE. For alkaline batteries, spongy zinc formation upon charging is a critical issue, which limits the lifetime. Many studies have been focused on the deposited morphology of zinc electrodes. Wen et al. [18] have studied lead ion and tetrabutylammonium bromide as additives for zinc deposition. But these additives usually increase the overpotential for zinc deposition and reduce the storage efficiency. Further, the hydrogen evolution is another issue especially under high current densities [19]. This evoluted gas reduces energy efficiency and makes zinc particles peeling off without reaction. That's why ZNBs are still operated at low current densities (below 20 mA cm^{-2}), which limits the power density and further development.

However, no study has successfully solved the two issues without compromising battery performances and environmental concerns. Three-dimensional porous nickel foams (NFs) have been widely used in batteries, electrochemical supercapacitors and fuel cells as the current collector and support matrix with open-pore structures and high specific surface areas [20–22]. The open-pore structure of three-dimensional electrode considerably reduces the internal resistance of the interface between electrode and electrolyte, and prevents zinc from falling before reacted. Their high specific surface is generally considered to reduce polarization with low realistic current density per geometrical area [23]. Therefore, three-dimensional NFs may be more suitable to act as negative electrodes for ZNBs, especially under high operated current densities. Whereas, according to the previous studies [24,25], as the three-dimensional porous electrodes usually have a considerable thickness, the potential distribution is non-uniform resulting in low utilization, it is of great importance to investigate the relationship between utilized electrode area, potential distribution and operated current density combined with battery performances.

In this work, we aimed at finding a more suitable negative electrode to improve the power density of ZNBs. Two types of nickel electrodes were tested to explore the relationship between electrode structure and battery performance. Furthermore, the relationship between utilized electrode area, potential distribution and operated current density was studied.

2. Experimental section

2.1. Electrochemical measurement

The electrochemical experiments were carried out in a conventional three-electrode cell using a CHI 612C potentiostat (Shanghai Chenhua Instrumental Co., Ltd., China). The working electrode was a piece of NF (3 × 5 × 2 mm, 110 pores per inch, 420 g m^{-2}, Changsha Lyrun Material Co., Ltd., China) or a piece of nickel sheet (NS) (3 × 5 × 0.1 mm, 890 g m^{-2}, Shanghai Jinchang Alloy Co., Ltd., China) with a sintered nickel hydroxide (10 × 10 × 0.7 mm, Jiangsu Highstar Battery Manufacturing, China) acting as the counter electrode. The reference electrode was an Hg/HgO electrode, which has a potential of 0.98 V vs. NHE. The NF and NS were degreased with acetone, etched with 6.0 mol dm^{-3} HCl for 10 min and rinsed thoroughly with deioned water. The electrolyte was 8.0 mol dm^{-3} KOH containing 0.4 mol dm^{-3} ZnO. All solutions were made with analytical grade chemical reagents and deioned water. The solutions were purged by bubbling ultra purity nitrogen stream for 30 min prior to measurements and maintained with a slight overpressure of nitrogen during the experiments. All potentials were referred to the reference electrode. Current densities were normalized to the geometrical area of working electrodes.

2.2. ZNB single cell test

The charge–discharge tests were conducted in a two-electrode cell constituted by a sintered nickel hydroxide positive plate (30 × 30 × 0.7 mm, area capacity, 25 mAh cm^{-2}) and a negative plate NF (30 × 30 × 2 mm) or NS (30 × 30 × 0.1 mm). The electrodes were pre-treated before test. The schematic diagram of cell structure was shown in Fig. 1. The interelectrode gap was 5 mm. The electrolyte was circulated through the cell and reservoir by a pump. Constant current charge–discharge tests were conducted by Arbin BT-2000 (Arbin Instruments, America). In order to avoid excessive gas evolution and degradation of electrode materials, the cell was charged to 80% of its full capacity based on the sintered nickel hydroxide electrode, and discharged at the same current density to 0.8 V. All above experiments were performed at room temperature.

2.3. Overpotential measurement

An Hg/HgO electrode was settled between positive and negative electrodes to monitor the variety of potentials on them using another two channels of Arbin BT-2000. The values were recorded every 5 s during the batteries' charge–discharge processes.

2.4. SEM characterization

The surface morphologies of deposited zinc were detected by scanning electron microscopy (SEM, JEOL JSM-6000, JEOL Ltd., Japan). Images were acquired using a 15 kV accelerating voltage. Negative electrodes after charging process were washed with deioned water and dry in a vacuum desiccator before test.

3. Results and discussion

3.1. Electrochemical performance

Electrochemical measurements are conducted to investigate zinc deposition/dissolution and hydrogen evolution on different

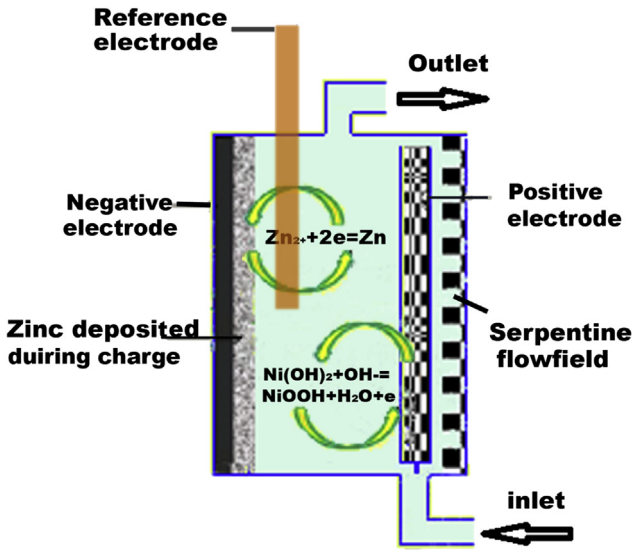

Fig. 1. Schematic diagram of cell structure.

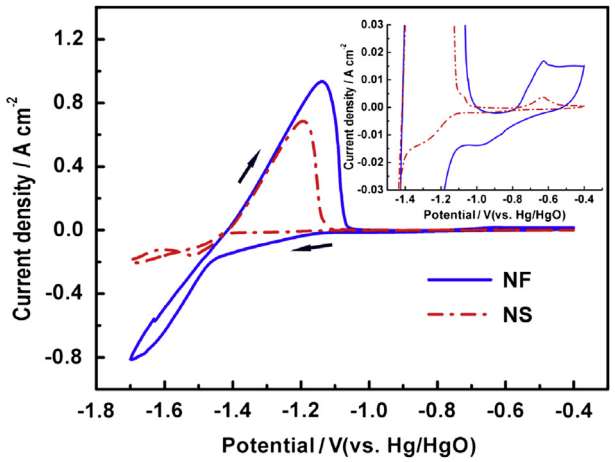

Fig. 2. Cyclic voltammograms of NS (red dash dot line) and NF (blue solid line) for zinc deposition and dissolution at a scan rate of 20 mV s^{-1}. (For interpretation of the references to colour in this figure legend, the reader is referred to the web version of this article.)

electrodes. Fig. 2 shows cyclic voltammograms (CVs) of NS and NF electrodes measured at a scan rate of 20 mV s^{-1}. An anodic peak is observed at about −0.63 V for both NS and NF which mainly associates with nickel redox in alkaline solution [26,27]. But the oxidation current peak area on NF is about 9 times higher than that on NS owing to its more active surface area [20]. When the potential is lower than −1.12 V, hydrogen gas starts to produce on the two electrodes, which not only reduces the current efficiency of zinc deposition, but also makes zinc falling before reacted. When the potential is lower than −1.42 V, zinc prefers to deposit on nickel substrates. Hydrogen evolution is inhibited with the increased zinc due to the high overpotential of hydrogen evolution on zinc. A cathodic current peak of zinc deposition is observed at −1.52 V on NS, while no cathodic current peak is appeared in the potential region on NF due to the high diffusion of zincate ions and hydrogen evolution. When further proceeds the cathode scan to more negative potential, hydrogen evolution remains the primary reaction. At the anodic proceeding, the anodic current peaks are observed at the potential between −1.1 V and −1.2 V both for NS and NF. As reported [28,29], the peak is associated with the dissolution of zinc ($Zn + 4OH^- \rightarrow [Zn(OH)_4]^{2-} + 2e$). However, the current peak on NF is only 1.4 times larger than that on NS, which is much lower than the active surface ratio. The above discussions indicate that NF provided more active surface for zinc deposition, but the inner pores may not be fully utilized.

Zinc dissolved behaviors on different structured electrode (NS and NF) are studied by cyclic voltammetry measured at various scan rates as shown in Fig. 3a and b. As soon as the zinc approaches to nil on the electrode, the anodic oxidation peak of zinc appears. With scan rates increasing, the anodic current peak is getting bigger and shifts to more positive potential. This phenomenon is usually observed in CV measurements for an electrochemical process due to the large overpotential for the reaction produced by slow electronic or ionic transport and sluggish charge transfer on the inner surface electrode and electrolyte. Fig. 3c and d indicates the relationship between dissolution rates of zinc and scan rates to determinate the reaction control step. Normally the reaction controlled by surface reaction (linear dependence, $i \propto \nu$) or diffusion limited mechanism (square-root dependence, $i \propto \nu^{1/2}$) could be distinguished by the responding current peak for various scan rates, where i is the current peak, ν is the scan rate as reported in literature [30,31]. And a mixed controlled can be existed as well. For NS, there is a square-root dependence between them, which indicates that the dissolution rate of zinc from NS is controlled by the diffusion of zincate ions from NS's surface. While, for NF, a linear dependence is observed when the scan rate is in the range of 10 mV s^{-1}–60 mV s^{-1}, which illustrates that the dissolution rate of zinc is controlled by surface reactions in this region. When the scan rate is higher than 60 mV s^{-1}, a deviation is observed due to the slow diffusion of zincate ions from the electrode surface or

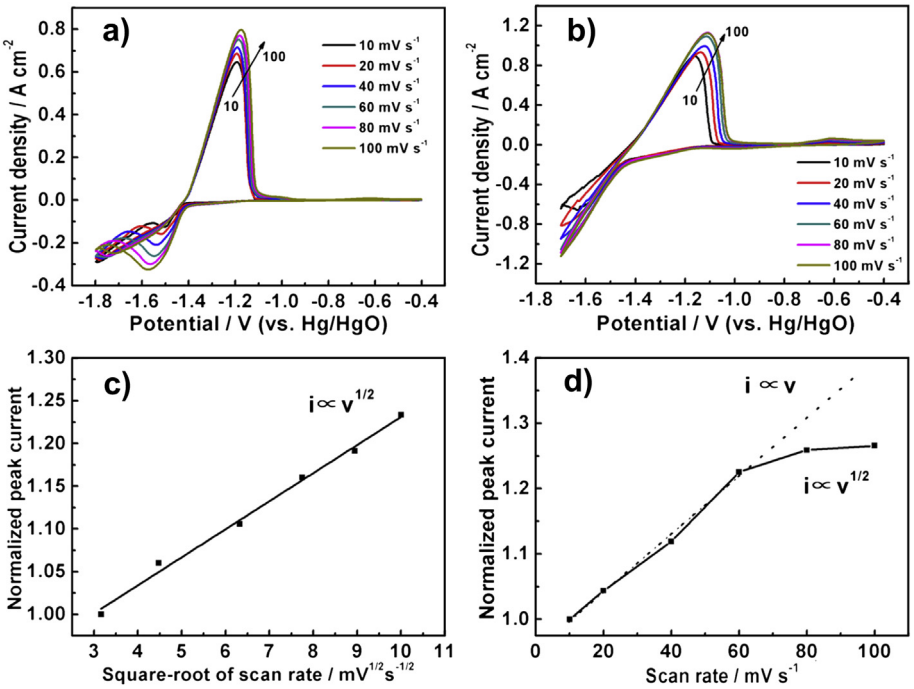

Fig. 3. Cyclic voltammograms of a) NS and b) NF for zinc deposition and dissolution at various scan rates (10 mV s^{-1}–100 mV s^{-1}) and dependence of normalized anodic peak current to the scan rate for c) NS and d) NF.

slow surface charge transfer. Thus, the dissolution of zinc from NF is more sensitive to scan rate, which could be more suitable used as negative electrodes for ZNBs under high operated current density.

Since any change in zinc deposited current indicates that a change in the active surface area, which associates with the surface morphology [18]. If the deposited zinc is uniform and compact, the real electrode surface area will not change, resulting in a constant current response under constant potential polarization. However, if the deposited zinc is sponges or dendrites, the real electrode surface area will drastically change, which results in greatly increase in the current response. The active surface change on NS and NF are investigated under a cathodic overpotential (50 mV) for 40 min as presented in Fig. 4a. It can be observed that the rise ratios in cathodic current on NS and NF electrodes are only 15.4% (from 25 mA cm^{-2} at 500 s to 29 mA cm^{-2} at 2400 s) and 12.8%. This may indicate that zinc deposited on two electrodes are both compact, which can be confirmed by the SEMs in Fig. 4b and c. The dendrites and sponges are not formed and the charge performance of the negative electrode would be excellent. But the NF provides a large space for zinc deposition. Zinc deposits not only on the surface, but also on the inner pores of NF as exhibited in Fig. 4c. Therefore, NF may be more suitable as substrates for zinc deposition in flowing alkaline zincate solution.

3.2. Charge–discharge performance

Based on the electrochemical performances of three-dimensional porous NF and flat NS for zinc deposition and dissolution defined in the previous section, the charge–discharge performances of single cells assembled with NS (cell 1) and NF (cell 2) are conducted using constant current charge–discharge tests under various current densities (20 mA cm^{-2}–80 mA cm^{-2}). The charge–discharge curves are shown in Fig. 5. A higher charge potential and a lower discharge potential are observed with the operated current density increasing from 20 mA cm^{-2} to 80 mA cm^{-2}, which indicates that the overpotential of single cells increased obviously during charge–discharge processes. There is a lower charge potential and a higher discharge potential for cell 2 compared to cell 1 at the current density from 40 mA cm^{-2} to 80 mA cm^{-2}. But an opposite phenomena occurs at the current density of 20 mA cm^{-2}, which may be due to non-uniform distribution of potentials on negative electrodes caused by ohmic loss. Large amount of hydrogen are produced on NFs, making it difficult for zinc to deposit. As a result, charge potential rise.

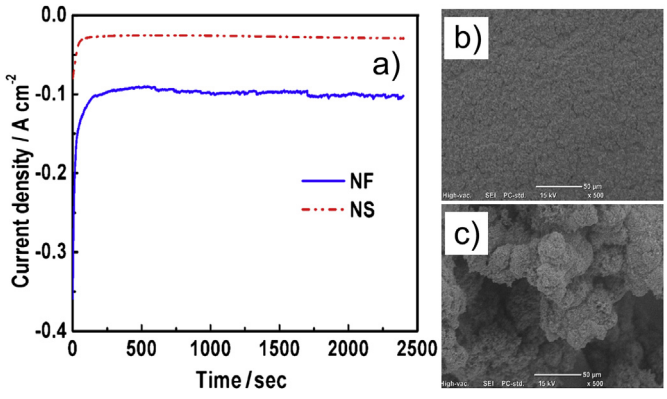

Fig. 4. a) Current-time curves at a constant cathodic overpotential (50 mV) for 40 min on NS (red dash dot line) and NF (blue solid line) and SEMs of zinc deposited on b) NS and c) NF. (For interpretation of the references to colour in this figure legend, the reader is referred to the web version of this article.)

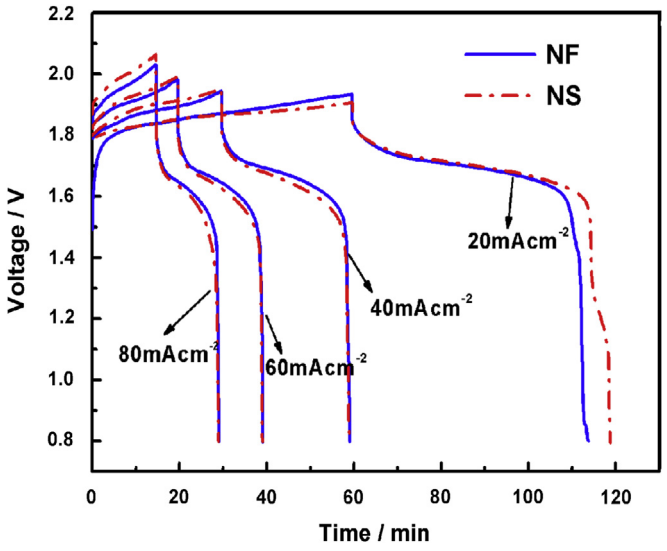

Fig. 5. Charge–discharge curves for ZNBs with NS (red dash dot line) and NF (blue solid line) as negative electrodes under different current densities. (For interpretation of the references to colour in this figure legend, the reader is referred to the web version of this article.)

The efficiencies of cell 1 and cell 2 are summarized in Fig. 6 including coulombic, voltage and energy efficiencies. The coulombic efficiency (CE) of cell 2 is much lower (89.5%) at 20 mA cm^{-2} due to gas evolution on electrodes resulting in a low energy efficiency (EE, 80.2%). At high current densities, cell 2 has slightly higher coulombic efficiencies than cell 1. And the voltage efficiency (VE) difference between cell 2 and cell 1 becomes larger with current density increasing, which results in better EE. For example, compared to cell 1, CE and VE of cell 2 are improved obviously to 97.3% and 82.1% resulting in the EE improved to 80.1% at 80 mA cm^{-2}. In summary, the cell assembled with NF shows better performance under high operated current densities.

3.3. Mechanism analyses

Due to the large surface, the realistic current density on NFs is low. Moreover, potential distribution on NFs may be not uniform

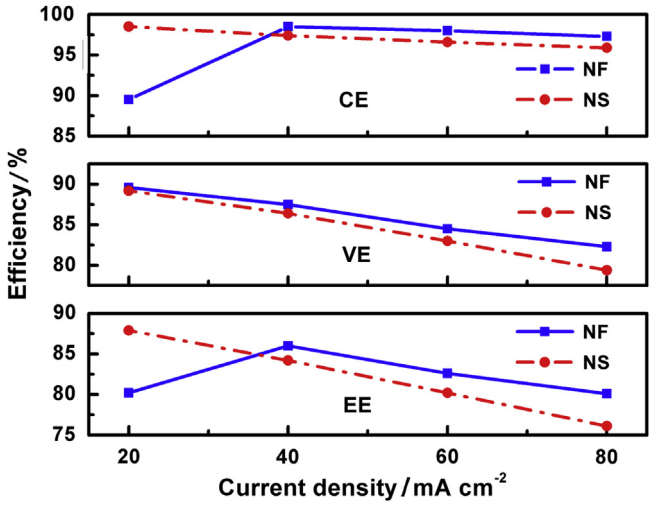

Fig. 6. Efficiencies of ZNBs assembled with NS (red dash dot line) and NF (blue solid line) under various current densities. (For interpretation of the references to colour in this figure legend, the reader is referred to the web version of this article.)

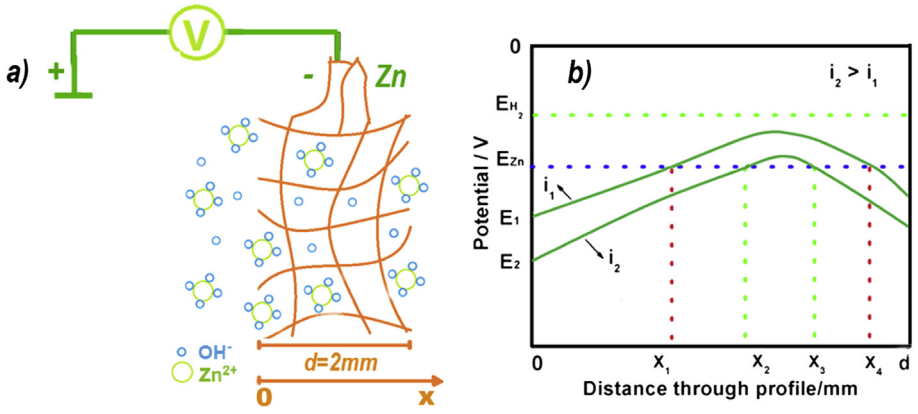

Fig. 7. a) The schematic of electrode position; b) potential distribution through the profile.

through profile according to the literature [32,33]. The schematic of electrode position and potential distribution in one dimensional direction are presented in Fig. 7. Where E_{H2} is the initial potential of hydrogen evolution, E_{Zn} is the initial potential of zinc deposition. When the potential is higher than E_{H2}, no reaction occurs on the NF. When the potential is between E_{H_2} and E_{Zn}, hydrogen is the only product produced on NF. When the potential is lower than E_{Zn}, there is a competition between zinc deposition and hydrogen evolution. However, due to the fact that zinc has a relatively high overpotential for hydrogen evolution, the rate of hydrogen evolution tends to be slower once the metallic zinc was deposited on the nickel substrate. At low current density, i_1 for instance, the efficient distance for zinc deposition is $X_1 + d - X_4$. At high current density (i_2), it shifts to $X_2 + d - X_3$, which increases the reacted area for zinc deposition and reduces the area for hydrogen evolution. This may explain why the cell assembled three-dimensional structure electrode has a slightly higher CE under high current density, but a lower CE under 20 mA cm^{-2}. The large utilized area also reduces the polarization of the negative electrode, result in a high VE.

In order to confirm our speculation, three-dimensional porous NFs are taken from the cell after charging under the current density of 20 mA cm^{-2} for 40 min and 40 mA cm^{-2} for 20 min. The zinc distribution on NFs is investigated by scanning electron microscopy, which reflects the potential distribution on porous electrodes. The results are presented in Fig. 8. It can be seen from Fig. 8a and b that most zinc deposited on the surface near the positive electrode ($X = 0$). There is little zinc deposited on the opposite side of NF ($X = d$), which indicates the non-uniform potential distribution. At a high current density (40 mA cm^{-2}), the quantity of zinc deposited on $X = 0$ decreases, while the quantity of zinc deposited on $X = d$ increases compared to 20 mA cm^{-2} as shown in Fig. 8c and d. This significantly confirms the potential distribution on porous electrodes described in Fig. 7.

For the ideal electrochemical systems, the electrode potential does not change during charge–discharge process. However, the electrode potential usually deviates from the equilibrium potential. The difference is overpotential, which indicates the degree of polarization associated with VE. The overpotential on

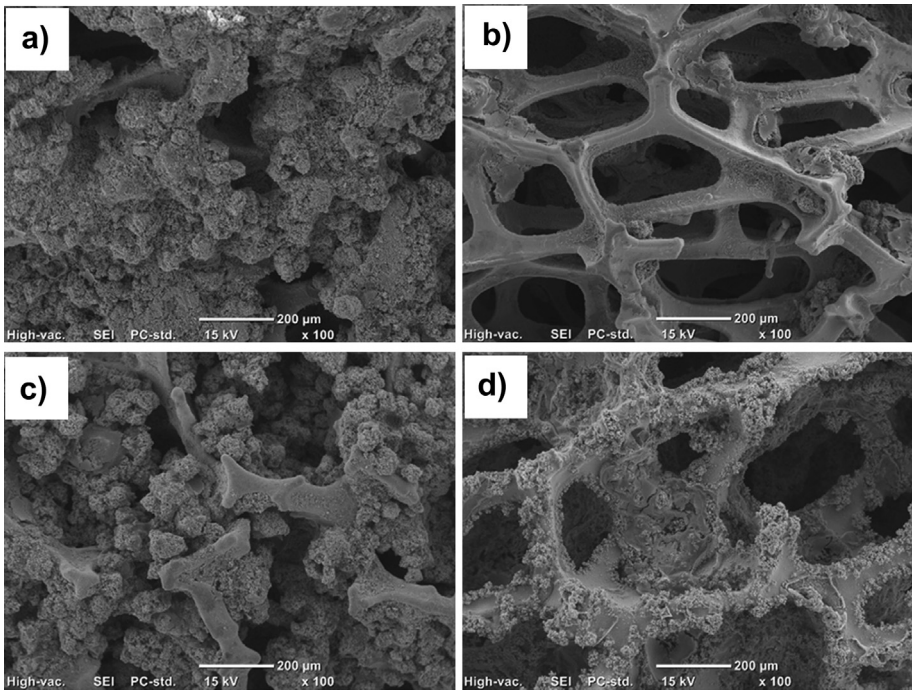

Fig. 8. SEMs of zinc deposited on NFs at 20 mA cm^{-2} for 40 min; a) $X = 0$, b) $X = d$; 40 mA cm^{-2} for 20 min, c) $X = 0$, d) $X = d$.

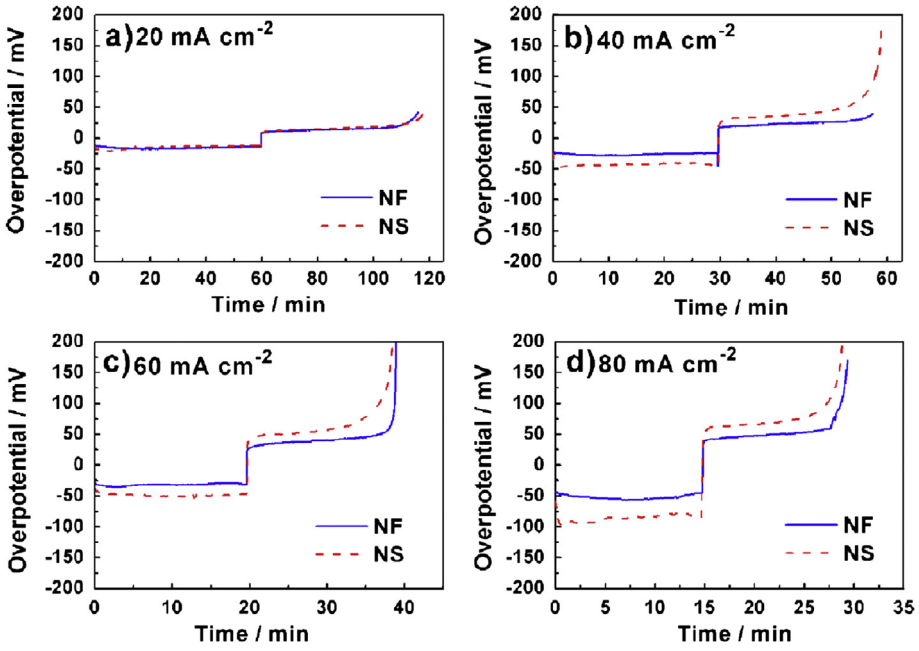

Fig. 9. Overpotentials responses vs. time on NS (red dash line) and NF (blue solid line) during charge–discharge under various current densities. (For interpretation of the references to colour in this figure legend, the reader is referred to the web version of this article.)

different electrodes is measured to investigate the polarization of negative electrodes. The results are shown in Fig. 9. The overpotentials on NS and NF both increase along with current density increasing from 20 mA cm^{-2} to 80 mA cm^{-2}. Three-dimensional porous NF can reduce the polarization of negative electrodes attributed to the large surface and open-pore structure. With the current density increasing, the overpotential difference between NS and NF is getting larger in both charge and discharge processes due to increasing utilized electrode area confirmed by Figs. 7 and 8, which further explains a high CE and VE on cell 2.

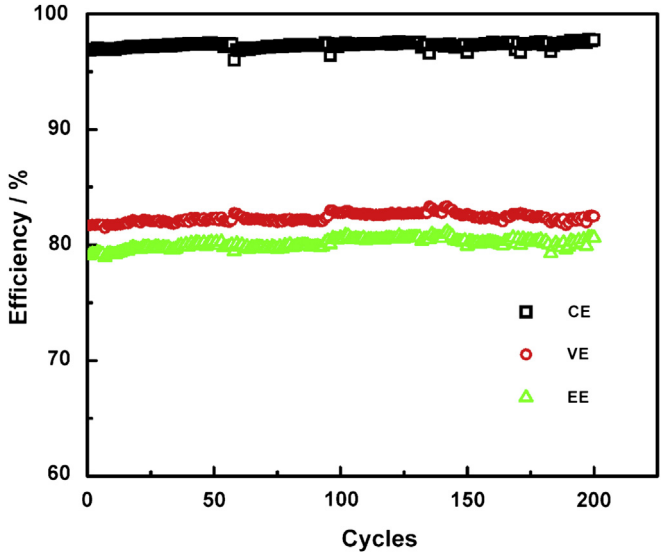

Fig. 10. Coulombic (dark square), voltage (red circularity), energy (green triangle) efficiencies of ZNB under 80 mA cm^{-2} over 200 cycles. (For interpretation of the references to colour in this figure legend, the reader is referred to the web version of this article.)

3.4. Cycle performance

The stability of ZNB assembled with three-dimensional NF as negative electrode is investigated via long charge–discharge cycles test at 80 mA cm^{-2} (Fig. 10). Both the efficiency and stability are improved considerably. A high CE (97.3%), VE (82.3%) and EE (80.1%) are obtained over 200 cycles without deterioration, which is the highest value ever reported in ZNBs.

3.5. Power density

As to most energy devices, the energy efficiency up to 80% is a basic requirement for commercial application, we attempt to increase the power density of ZNBs with energy efficiency higher than 80%. In order to calculate the power density, detailed description of the single cell components is summarized in Table 1. The power density is calculated by the following equation:

$$P = \frac{IV}{m_+ + m_- + m_e} \quad (1)$$

The average output voltage is 1.62 V at 0.72 A (80 mA cm^{-2}, 9 cm^2). The mass includes a positive electrode, a negative electrode and the electrolyte. Since the mass of the positive and negative electrodes are much lower than the electrolyte. The electrolyte is

Table 1
Parameters in battery for power density calculation.

Items	Values	
Output current (I)/A	0.72	0.72
Average output voltage (V)/V	1.62	1.62
Mass of positive electrode (m_+)/g	2.2	2.2
Mass of negative electrode (m_-)/g	0.42	0.42
Mass of electrolyte (m_e)/g	11.5	16.4
Utilization of electrolyte/%	100	70
Power density (P)/W kg^{-1}	83	61

the largest contributor to the total mass. The power density can reach to 83 W kg^{-1} with 100% utilization of the electrolyte, which is nearly four times higher than the present ZNBs (1.65 V at 20 mA cm^{-2}). Even if the electrolyte utilization is 70%, the power density still reaches up to 61 W kg^{-1}.

4. Conclusions

Three-dimensional porous NFs are first introduced to ZNBs to decrease the overpotential of the negative electrode. The NF shows excellent electrochemical property for zinc deposition and dissolution. Under high current density, the NF with a large utilized electrode area shows a low polarization resulting in a high CE and VE. Both the efficiency and stability are considerably improved. A high CE (97.3%) and EE (80.1%) are obtained with NF as negative electrodes under 80 mA cm^{-2} over 200 cycles, which is the highest value ever reported. The power density is improved four times to 83 W kg^{-1}, which improves the response for energy conversion and reduces the cost significantly. The high power density ZNB will arouse a new revolution in FBs combined with its advantages of high energy density, low cost and non-toxic.

Acknowledgments

This work is financially supported by the National Basic Research Program of China (973 Program No. 2010CB227204).

References

[1] F. Díaz-González, A. Sumper, O. Gomis-Bellmunt, R. Villafáfila-Robles, Renewable Sustainable Energy Rev. 16 (2012) 2154–2171.
[2] B. Dunn, H. Kamath, J.M. Tarascon, Science 334 (2011) 928–935.
[3] Y. Gogotsi, P. Simon, Science 334 (2011) 917–918.
[4] J.R. Miller, Science 335 (2012) 1312–1313.
[5] C. Ponce de León, A. Frías-Ferrer, J. González-García, D.A. Szánto, F.C. Walsh, J. Power Sources 160 (2006) 716–732.
[6] J. Leadbetter, L.G. Swan, J. Power Sources 216 (2012) 376–386.
[7] R.F. Savinell, J. Electrochem. Soc. 126 (1979) 357.
[8] D.A. Johnson, J. Electrochem. Soc. 132 (1985) 1058.
[9] H.S. Lim, J. Electrochem. Soc. 124 (1977) 1154.
[10] Y. Xu, Y.-H. Wen, J. Cheng, G.-P. Cao, Y.-S. Yang, Electrochim. Acta 55 (2010) 715–720.
[11] M. Skyllas-Kazacos, J. Electrochem. Soc. 134 (1987) 2950.
[12] H. Zhang, H. Zhang, X. Li, Z. Mai, W. Wei, Energy Environ. Sci. 5 (2012) 6299.
[13] P. Zhao, H. Zhang, H. Zhou, B. Yi, Electrochim. Acta 51 (2005) 1091–1098.
[14] D. Pletcher, R. Wills, J. Power Sources 149 (2005) 96–102.
[15] J. Cheng, L. Zhang, Y.-S. Yang, Y.-H. Wen, G.-P. Cao, X.-D. Wang, Electrochem. Commun. 9 (2007) 2639–2642.
[16] C. Ponce de León, F.C. Walsh, Secondary batteries – zinc systems|zinc–bromine, in: G. Jürgen (Ed.), Encyclopedia of Electrochemical Power Sources, Elsevier, Amsterdam, 2009, pp. 487–496.
[17] L. Zhang, J. Cheng, Y. Yang, Y. Wen, X. Wang, Z. Xie, Electrochemistry 14 (2008) 248–252.
[18] Y. Wen, T. Wang, J. Cheng, J. Pan, G. Cao, Y. Yang, Electrochim. Acta 59 (2012) 64–68.
[19] Y. Ito, M. Nyce, R. Plivelich, M. Klein, S. Banerjee, J. Power Sources 196 (2011) 6583–6587.
[20] M. Grdeń, M. Alsabet, G. Jerkiewicz, ACS Appl. Mater. Interfaces 4 (2012) 3012–3021.
[21] W. Xing, S. Qiao, X. Wu, X. Gao, J. Zhou, S. Zhuo, S.B. Hartono, D. Hulicova-Jurcakova, J. Power Sources 196 (2011) 4123–4127.
[22] F. Bidault, D.J.L. Brett, P.H. Middleton, N. Abson, N.P. Brandon, Int. J. Hydrogen Energy 34 (2009) 6799–6808.
[23] R. Pollard, J. Newman, Electrochim. Acta 25 (1980) 315–321.
[24] K. Scott, P. Argyropoulos, J. Electroanal. Chem. 567 (2004) 103–109.
[25] J.J. Hwnag, W.R. Chang, R.G. Peng, P.Y. Chen, A. Su, Int. J. Hydrogen Energy 33 (2008) 5718–5727.
[26] S.L. Medway, C.A. Lucas, A. Kowal, R.J. Nichols, D. Johnson, J. Electroanal. Chem. 587 (2006) 172–181.
[27] A.A. Wronkowska, Surf. Sci. 214 (1989) 507–522.
[28] J.O.M. Bockris, Z. Nagy, A. Damjanovic, J. Electrochem. Soc. 119 (1972) 285.
[29] D.D. Macdonald, K.M. Ismail, E. Sikora, J. Electrochem. Soc. 145 (1998) 3141–3149.
[30] H. Zhou, M. Xu, Q. Huang, Z. Cai, W. Li, J. Appl. Electrochem. 39 (2009) 1739–1744.
[31] J.-H. Kim, K.J. Kim, M.-S. Park, N.J. Lee, U. Hwang, H. Kim, Y.-J. Kim, Electrochem. Commun. 13 (2011) 997–1000.
[32] R. Reddy, R.G. Reddy, Electrochim. Acta 53 (2007) 575–583.
[33] T. Doherty, J.G. Sunderland, E.P.L. Roberts, D.J. Pickett, Electrochim. Acta 41 (1996) 519–526.